T. Bierkandt, P. Hemberger, P. Oßwald, D. Krüger, M. Köhler, T. Kasper, Flame structure of laminar premixed anisole flames investigated by photoionization mass spectrometry and photoelectron spectroscopy, Proceedings of the Combustion Institute 37 (2019) 1579-1587.

The original publication is available at www.elsevier.com

https://doi.org/10.1016/j.proci.2018.07.037

Flame structure of laminar premixed anisole flames investigated by photoionization mass spectrometry and photoelectron spectroscopy

Thomas Bierkandt[1,3*], Patrick Hemberger[2], Patrick Oßwald[3], Dominik Krüger[3], Markus Köhler[3], Tina Kasper[1]

[1]Mass Spectrometry in Reactive Flows – Thermodynamics, IVG, University of Duisburg-Essen, 47057 Duisburg, Germany

[2]Molecular Dynamics Group, Paul Scherrer Institute, 5232 Villigen PSI, Switzerland

[3]Institute of Combustion Technology, German Aerospace Center (DLR), Pfaffenwaldring 38-40, 70569 Stuttgart, Germany

*Corresponding Author: Thomas Bierkandt, German Aerospace Center, Pfaffenwaldring 38-40, 70569 Stuttgart, Germany
phone: +49-711-6862-8178, fax: +49-711-6862-578
email: thomas.bierkandt@dlr.de

Colloquium Topic Area: **Laminar Flames,**
Reaction Kinetics (alternative session)

Word counts (method 1)

Part	Method	# words
Abstract	Microsoft Word 2010 word count	287
Main text	Microsoft Word 2010 word count	4387
Equations	No equations	0
Nomenclature	No nomenclature	0
References	(34 + 2) × 2.3 lines/ref × 7.6 words/line	629
Tables	No tables	0
Figure 1	[(50.0 mm + 10 mm) × 2.2 words/mm × 1] + 32	164
Figure 2	[(100 mm + 10 mm) × 2.2 words/mm × 2] + 20	504
Figure 3	[(101.3 mm + 10 mm) × 2.2 words/mm × 2] + 23	516
Total (excl. abstract)		**6200**

Supplementary Material has been included in the submission of this paper

Submitted to the 37th International Symposium on Combustion, Dublin, 2018

Color figures in electronic version only

Abstract

Two laminar, premixed, fuel-rich flames fueled by anisole-oxygen-argon mixtures with the same cold gas velocity and pressure were investigated by molecular-beam mass spectrometry at two synchrotron sources where tunable vacuum-ultraviolet radiation enables isomer-resolved photoionization. Decomposition of the very weak O–CH_3 bond in anisole ($C_6H_5OCH_3$) by unimolecular decomposition yields the resonantly-stabilized phenoxy radical (C_6H_5O). This key intermediate species opens reaction routes to five-membered ring species, such as cyclopentadiene (C_5H_6) and cyclopentadienyl radicals (C_5H_5). Anisole is often discussed as model compound for lignin to study the phenolic-carbon structure in this natural polymer. Measured temperature profiles and mole fractions of many combustion intermediates give detailed information on the flame structure. A very comprehensive reaction mechanism from the literature which includes a sub-scheme for anisole combustion is used for species modeling. Species with the highest measured mole fractions (on the order of 10^{-3}–10^{-2}) are CH_3, CH_4, C_2H_2, C_2H_4, C_2H_6, CH_2O, C_5H_5 (cyclopentadienyl radical), C_5H_6 (cyclopentadiene), C_6H_6 (benzene), C_6H_5OH (phenol), and C_6H_5CHO (benzaldehyde). Some are formed in the first destruction steps of anisole, e.g., phenol and benzaldehyde, and their formation will be discussed and with regard to the modeling results. There are three major routes for the fuel destruction: (1) formation of benzaldehyde (C_6H_5CHO), (2) formation of phenol (C_6H_5OH), and (3) unimolecular decomposition of anisole to phenoxy (C_6H_5O) and CH_3 radicals. In the experiment, the phenoxy radical could be measured directly. The phenoxy radical decomposes via a bicyclic structure into the soot precursor C_5H_5 and CO. Formation of larger oxygenated species was observed in both flames. One of them is guaiacol (methoxyphenol), which decomposes into fulvenone. The presented speciation data, which contain more than 60 species mole fraction profiles of each flame, give insights into the combustion kinetics of anisole.

Keywords: Anisole; Biomass; Biofuel; Oxygenated species; PEPICO

1. Introduction

A significant source of biofuel production is biomass yielding typical oxygenated biofuels like ethanol or butanol. Depending on the source of the biomass, it mainly consists up to 90% of cellulose, hemicellulose, and lignin in different amounts [1]. Lignin is a strongly cross-linked polymer consisting of aromatic alcohols. There are three main components, the so-called monolignol monomers *p*-coumaryl, coniferyl, and sinapyl alcohol, which describe the structure of lignin (see Fig. S1 in the Supplementary Material). In chemical terms, lignin has a phenolic structure and the simplest compounds which mirror this structure and are derived from lignin are phenol (C_6H_5OH), anisole ($C_6H_5OCH_3$), and guaiacol ($HOC_6H_4OCH_3$). They are important model compounds for lignin to study the combustion properties of the phenolic-carbon structure. The soot precursor cyclopentadienyl radical can be formed early in the flame by the decomposition of the phenoxy radical and gives access to five-membered ring species and to polycyclic aromatic hydrocarbons.

Several studies on the pyrolysis and oxidation of anisole already exist but the combustion of anisole in flames has not been investigated yet. Anisole is not a typical biofuel because of its aromatic character. Only few studies are concerned with aromatic biofuels because of strict emission limits for benzene and the fact that most of benzene emissions originate from exhaust gases of gasoline engines. Lignin is the second-most naturally occurring polymer and some toxicologically harmless aromatics could be produced from biomass by hydrothermal liquefaction and solvolysis [2]. A current overview on the investigation of engine combustion of anisole-blended fuels is summarized in [2]. For example, Zhou et al. [3] have shown that the efficiency of a diesel engine increases with simultaneously lower exhaust emissions if an anisole-blended diesel (10% by volume) is used instead of the neat diesel fuel. A new study by Tian et al. [4] deals with lignin-based aromatics as potential antiknock additives in Otto engines. Anisole increases the octane number of a commercial gasoline, but is not as effective as toluene.

There are some studies on the reactivity and the chemical decomposition during the pyrolysis and oxidation of anisole. For example, Mulcahy et al. [5] have investigated the kinetics of the reaction of anisole with methyl radicals between 453 and 539 K and 10–30 Torr. At 487 K the hydrogen abstraction at the aromatic ring of the anisole leading to the formation of methoxyphenyl radicals is 12 times slower than the formation of the phenoxymethyl radicals by abstraction of a hydrogen atom at the methyl group. The pyrolysis of anisole was also studied by Schlosberg et al. [6] at 450 °C in an autoclave. Major products were phenol, methane, CO, benzaldehyde, polyphenyls, and polyethers. Initiation of thermal decomposition of anisole is followed by formation of phenoxy and methyl radicals. Lin and Lin [7, 8] studied the unimolecular decomposition of anisole to cyclopentadienyl radicals and CO in the range of 1000–1580 K and 0.4–0.9 atm and determined a rate constant for this reaction. For low temperatures, they suggested the formation of *ortho*- and *para*-cresols which are both isomers of anisole. In the study of Mackie et al. [9], the reaction rate of the unimolecular decomposition of anisole to phenoxy and methyl radicals was determined from the pyrolysis of anisole at 850–1000 K and 0.16–1.2 atm. They also found that most of the oxygen is bound in the pyrolysis products phenol and cresol and not in CO. Arends et al. [10] have investigated the thermolysis of anisole in a hydrogen atmosphere in a flow reactor at 793–1020 K and developed a reaction mechanism for the thermolysis. A first reaction mechanism for the pyrolysis of anisole was developed by Pecullan et al. [11] and was validated against pyrolysis and oxidation experiments in a flow reactor at atmospheric pressure and 1000 K. At these conditions, differences between the oxidation and the pyrolysis are marginal. In the study of Scheer et al. [12], propargyl radicals were identified as products in the pyrolysis of anisole up to 1300 °C but the formation of benzene takes place by decomposition of methylcyclopentadienes. A detailed kinetic study of the pyrolysis and oxidation of anisole in a jet-stirred reactor was performed at 673–1173 K by Nowakowska et al. [13]. They also developed a very comprehensive reaction mechanism with 303 species and 1922 reactions based on the oxidation mechanism of ethylbenzene by Husson et al. [14]. The main decomposition occurs by formation of phenoxy radicals and stable main products are phenol, methane, CO,

benzene, and hydrogen. The pyrolysis of anisole behind reflected shock waves was investigated by Shu et al. [15] between 1000 and 1270 K and 1.3–1.6 bar. Recently, Wagnon et al. [16] have investigated the pyrolysis and oxidation (stoichiometries of 0.5, 1, and 2) of anisole in a jet-stirred reactor at atmospheric pressure and 675–1275 K and developed a new anisole mechanism.

The investigation of the combustion of the lignin model compound anisole is a first step to understand the chemical reactions of the methoxyphenol destruction and the formation of important intermediate species in laminar, premixed flames. Additionally, the formation of soot precursors is of crucial interest because methoxyphenols are important precursors for the formation of polycyclic aromatic hydrocarbons which are formed during the combustion of biomass and biomass gasification [13]. A deeper understanding of intermediate species formation can help to understand the origin of harmful emissions during wood combustion and to reduce tar formation during biomass gasification.

2. Experiment

Two laminar, premixed, fuel-rich anisole flames were investigated at 40 mbar. One flame with a stoichiometry of 1.2 was measured at the Advanced Light Source (ALS) in Berkeley, USA, while the richer flame (Φ=1.6) was investigated at the Swiss Light Source (SLS) in Villigen, Switzerland. Both anisole-O_2-Ar-flames have a cold gas velocity of 65.2 cm/s at 300 K and 40 mbar with 50% argon dilution and a total gas flow of 4 slm. The diameter of the water-cooled sintered matrix of the burner was 6 cm. In both experiments, vacuum-ultraviolet (VUV) synchrotron radiation provides soft ionization and a molecular-beam mass spectrometry (MBMS) setup is used for identification and quantification of combustion intermediates formed during the combustion of anisole. Molecular-beam sampling preserves the gas composition during the sampling process and enables even the detection of radicals. Collisionless free-molecular flow is reached very fast by this sampling procedure [17] and a chemical composition shift after sampling is only minor [18]. Main differences between the two setups are related to the spectrometers. The instrument at the ALS provides a high-resolution reflectron time-of-flight mass spectrometer ($m/\Delta m$>3000). This enables the determination

of the elemental composition (e.g., separation of propene and ketene on mass 42). At the SLS a photoelectron photoion coincidence (PEPICO) spectrometer enables simultaneous detection of ions and electrons formed in the ionization event. This feature can be helpful for isomer identification, especially if three or more isomers are present [19]. More detailed information about the ALS and SLS instruments can be found in [20] and [21], respectively. Data evaluation follows the procedure of Cool et al. [20] with modifications for the measurements at the SLS described in [22] and a detailed description is also offered in the Supplementary Material.

The temperature of the exhaust gas in the flame was measured with a platinum-rhodium-alloy thermocouple coated with Al_2O_3 to minimize catalytic effects. The temperature profile was calculated from the temperature dependence of the sampling rate, determined by the pressure in the intermediate or ionization chamber [23]. A temperature profile obtained by this procedure takes perturbation by the sampling nozzle into account. The uncertainty of the temperature profiles is expected to be 5–10%. Some additional information about the temperature profile calculations is provided in the Supplementary Material.

The pressure of the burner chamber was set to 40 ± 0.1 mbar by a throttle valve. Gas flows were metered by thermal mass flow controllers with an accuracy of ± 1%. The liquid fuel anisole (Sigma-Aldrich, 99.7%) is pumped by a HPLC pump at the SLS and a syringe pump at the ALS and vaporized in self-made vaporizer systems. The flow accuracy of the pumps is ± 1% for the HPLC pump and ± 0.5% for the syringe pump. The uncertainty of the calculated mole fractions is estimated to be 15–20% for main species and 30–50% for intermediate species with measured photoionization cross sections [24]. For species with unknown photoionization cross sections like most radicals, the uncertainty of the mole fraction can increase to a factor of 2-4. Additional information about the measurement uncertainties is given in the Supplementary Material.

3. Results

Detailed isomer-resolved speciation data is presented to give insights into the combustion kinetics of anisole in laminar premixed flames under fuel-rich conditions. A comprehensive reaction mechanism for the combustion of hydrocarbon and oxygenated fuels from Ranzi et al. [25] was used to simulate species mole fractions with the burner-stabilized flame reactor module of the Chemical Workbench (Kintech Lab) [26] considering thermodiffusion. This mechanism includes a sub-scheme for the oxidation and combustion of anisole [27] and further species released from biomass pyrolysis [28]. Experimentally determined temperature profiles were used for the simulation and neither modeled nor experimental mole fraction profiles were shifted. For both flames the modeling results as well as the experimental mole fraction profiles are provided as Supplementary Material. Formation of combustion products formed from the fuel is discussed in detail relating to the modeling results.

3.1 Mole fraction profiles of the main species

Comparison of experimentally determined mole fractions with simulated mole fraction profiles of all main species, that is, Ar, CO, CO_2, H_2, H_2O, O_2, and anisole, indicate if the reaction mechanism can predict the global anisole combustion chemistry for the investigated conditions. As seen from Fig. 1, good agreement between the experimental data and the modeling results is reached for the main species of the flame with a stoichiometry of 1.6. Clearly recognizable deviations in the exhaust gas region for CO and H_2O are within the error margins mentioned above. The shape of the mole fraction profiles in the reaction zone close to the burner is also reproduced very well by the model. Similar observations are made for the flame with Φ=1.2 measured at the ALS (see Fig. S2 in the Supplementary Material). Differences are again within the error margin. At Φ=1.2, oxygen is not totally consumed as predicted by the model, but in comparison to the experiment fuel and oxygen consumption are slightly faster in the simulation.

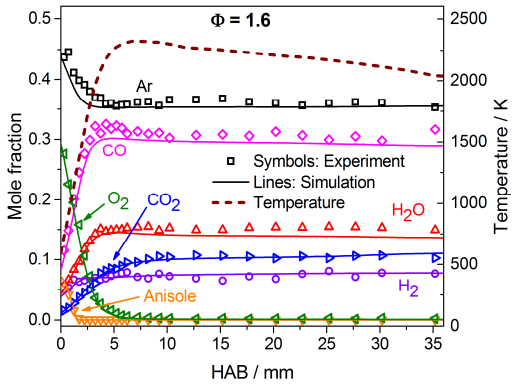

Fig. 1. Main species mole fractions and temperature profile of the anisole flame with stoichiometry of 1.6 measured at the SLS. Symbols: experimental data; solid lines: modeling results; dashed line: temperature profile.

3.2 Anisole destruction steps

A stringent test to verify a kinetic mechanism is the comparison of mole fraction profiles of intermediate species, especially species involved in the main consumption pathway of the fuel. Reaction path analyses of both flames illustrate the primary consumption pathways of anisole and give an overview of important combustion intermediates. The reaction pathways of the carbon flux in the entire flames are shown in Fig. 2. Only carbon fluxes higher than 10% are shown. Thickness of arrows represents the carbon flux and indicates the main consumption pathway. Percentages next to arrows give the contribution of individual destruction rates of a species. Chemical structures of some species shown in the reaction path are given in Table S1.

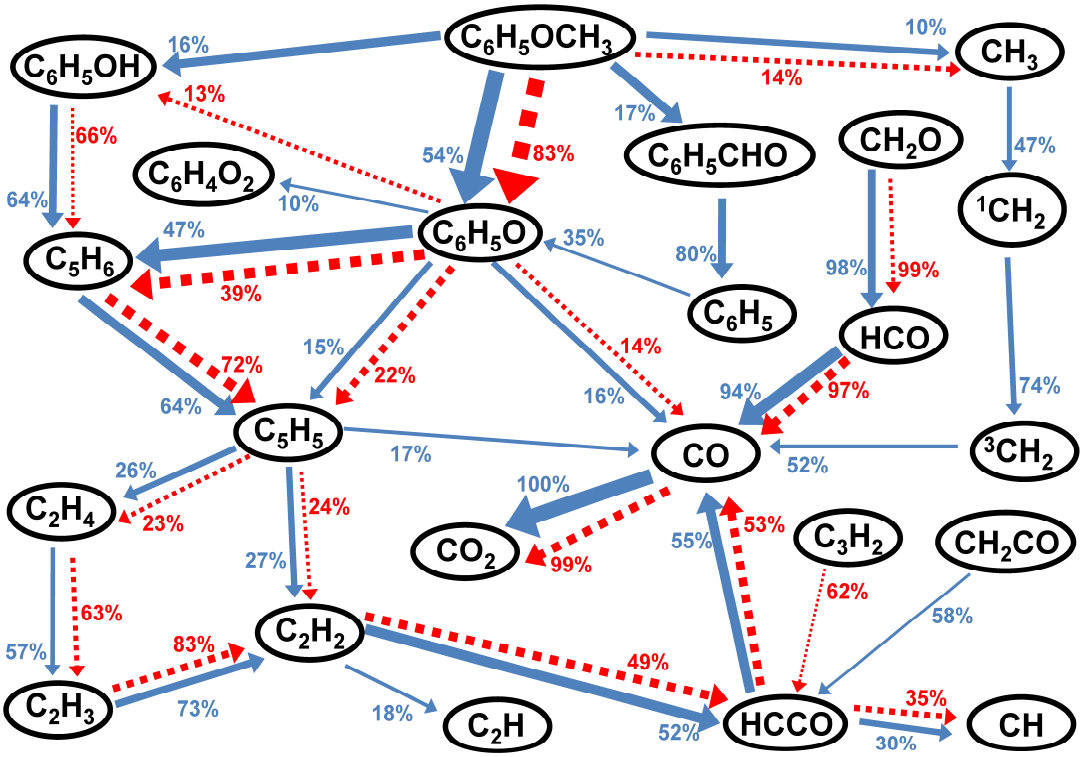

Fig. 2. Reaction pathways of total carbon flux in the entire flames. Solid arrows (blue): Φ=1.2; dashed arrows (red): Φ=1.6.

As seen from Fig. 2, three main destruction steps of anisole ($C_6H_5OCH_3$) take place: (1) formation of benzaldehyde from reaction of $C_6H_5OCH_3$ with H (33%), OH (58%), and O (9%) radicals, (2) formation of phenol from reaction of $C_6H_5OCH_3$ with H (42%) and *ipso* addition of OH (58%) radicals, and (3) unimolecular scission of the O–CH_3 bond in the methoxy group to yield phenoxy (C_6H_5O) and methyl (CH_3) radicals. The latter reaction should be strongly favored regarding the bond dissociation energies in anisole (see Fig. S3 in the Supplementary Material) because the dissociation energy of the O–CH_3 bond is with only 63.2 kcal/mol 45% smaller than the dissociation energy of the C–H bond in the methyl group [13]. While in the leaner flame the two first-mentioned formation pathways count for one third of the decay rate of consumption of anisole, the formation of phenoxy is distinctly preferred in the richer flame. Formation of phenoxy radicals is also more important for fuel-rich conditions in the anisole mechanism of Wagnon et al. [16]. Fuel destruction to benzaldehyde and further destruction of intermediate species are initiated mainly by the small

radicals H, O, and OH. At the SLS, H and OH radicals could be directly measured while O and OH were measured at the ALS. To obtain reliable mole fractions, the concentrations of these radicals were calculated from partial equilibrium and the measured signal profiles [17]. Calculated mole fractions by this method show good agreement with the simulation results as seen in Fig. S4.

Depending on the flame position and temperature, the ratio of phenoxy + CH_3 to benzaldehyde and phenol, respectively, is different. Figure S5 shows reaction pathways of carbon flux for two positions in the richer flame. At 0.9 mm (≈1050 K) benzaldehyde and phenol are mainly formed from anisole, while further downstream the formation of the phenoxy radical is dominating, for example, at 1.7 mm (≈1470 K). Nowakowska et al. [13] observed similar results in the oxidation of anisole in a jet-stirred reactor where the formation of the phenoxy radical by unimolecular decomposition was the dominating destruction path of anisole at higher temperatures while at lower temperatures also the formation of the anisyl radical ($C_6H_5OCH_2$) by hydrogen abstraction became relevant. Phenoxy radicals are resonantly stabilized and are expected in higher concentrations in comparison to more reactive radicals [11]. In both flames, the phenoxy and methyl radicals obtained from unimolecular bond breaking of the methoxy group in anisole could be measured directly as well as their combustion products phenol (C_6H_5OH), cyclopentadienyl radical (C_5H_5), and formaldehyde (CH_2O). Hydrogen abstraction at the methyl group of anisole would result in the formation of the anisyl radical ($C_6H_5OCH_2$) [5], which was not detectable in the flames. The anisyl radical isomerizes by *ipso* rearrangement and following β-scission yields benzaldehyde (C_6H_5CHO) [6]. In the mechanism, benzaldehyde is directly formed from anisole by hydrogen abstraction in one step and was found in high concentrations. In the stoichiometric oxidation of anisole in a jet-stirred reactor, benzaldehyde was formed at the lowest temperatures [13]. H-abstraction at the aromatic ring of anisole (i.e., formation of methoxyphenyl radicals) plays no role [5] and is also not considered in the reaction mechanism.

Figure 3 compares mole fractions of species that are involved in the early destruction of anisole and are also found in high concentrations (on the order of 10^{-3}–10^{-2}) in the experiment. Estimated

errors of 50% are added as areas above and below the experimental mole fraction values. As mentioned in Section 2, the error of species with unknown photoionization cross section (e.g., phenoxy radicals) can also be higher but is not shown for reason of better clarity. Some more species mole fractions are given in Fig. S6. Regarding the uncertainty of the calculated mole fraction profiles, good agreement for absolute mole fractions of most intermediate species and profile shapes between experimental values and the modeling results is observed. The peak maxima are well predicted for the richer flame, while the peak maxima for the flame with Φ=1.2 are shifted closer to the burner in the simulation. The ratios between the Φ=1.2 and 1.6 flames are very well predicted by the model.

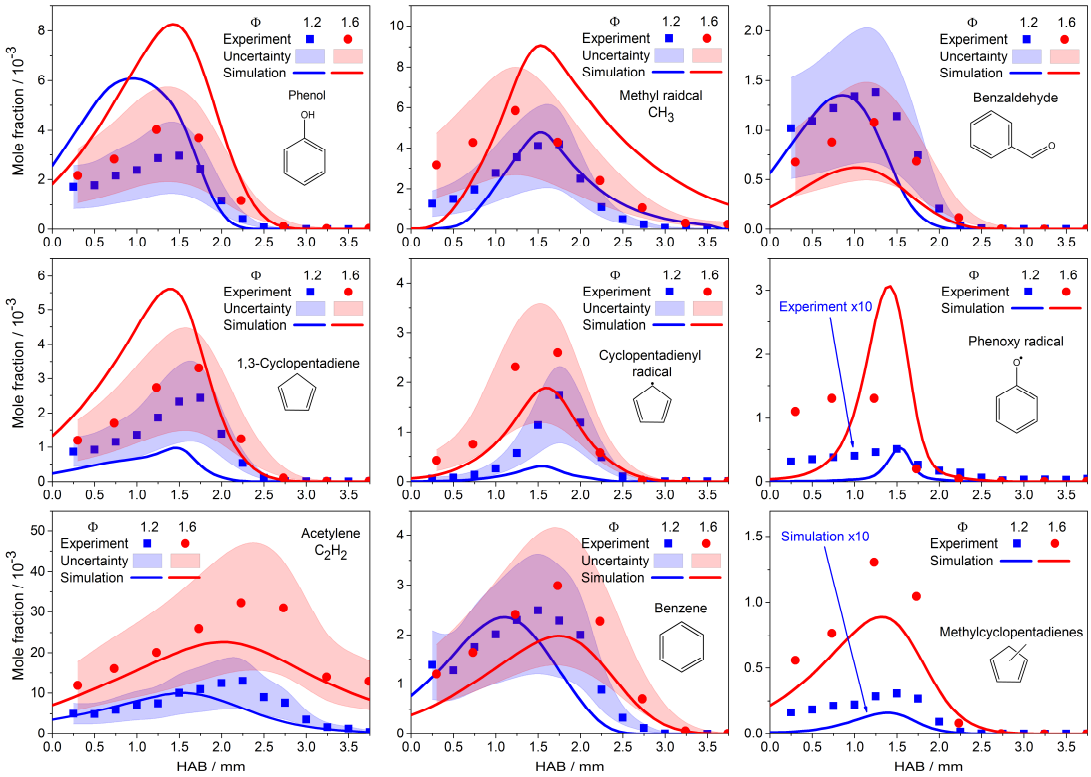

Fig. 3. Mole fraction profiles of some stable intermediate and radical species founded in higher concentration. Symbols: experimental data; solid lines: modeling results.

The detection of the phenoxy radical was possible in both flame experiments, but the measured mole fraction is distinctly smaller (more than one order of magnitude) for the leaner flame. In the

richer flame, the simulation overpredicts the peak mole fraction of phenoxy by a factor of two. Because the mole fraction was calculated from scans at nearly the same photon energy (9 and 9.05 eV), the difference cannot result from the estimated photoionization cross section. We used a value of 4 Mb which was calculated by linear interpolation between the recently determined absolute photoionization cross section of the phenoxy radical at 10.486 eV by Xu et al. [29] and the value of 0 Mb at the ionization energy of the phenoxy radical (8.56 eV). Methyl radical formation is directly coupled to the unimolecular decomposition of anisole, but the mole fractions are well predicted by the simulation for both flames, especially for the flame with the lower phenoxy radical concentration. One explanation is that different sampling effects of the two different systems (e.g., different sampling nozzle designs and different sampling lengths) could account for the radical loss. The system at the SLS is very sensitive for radical detection [22]. Experimental mole fraction profiles of phenoxy are relatively broad and imply that phenoxy radical formation is also relevant at lower temperatures closer to the burner, while the simulated phenoxy profiles are very narrow in comparison to the experiments and other intermediate profiles from the simulation.

It is well-known that phenoxy decomposes unimolecularly into cyclopentadienyl radicals (C_5H_5) and CO via a bicyclic structure [30] (see Fig. S7). Consumption of the phenoxy radical occurs also by the formation of 1,3-cyclopentadiene (C_5H_6) and CO and by hydrogen addition in a three-body reaction to yield phenol ($H + C_6H_5O + M = C_6H_5OH + M$). As shown in Fig. 3, the five-membered ring species cyclopentadienyl and cyclopentadiene are obtained in higher concentrations for the richer flame in accordance with the modeling results, but the experimentally observed differences between the two equivalence ratios are not as big as in the modeling predictions. In the leaner flame, experimental peak mole fractions of C_5H_5 and C_5H_6 are 5.8 and 2.5 times higher, respectively, than the modeling results. The distinctly higher mole fraction of the cyclopentadienyl radical in the leaner flame fits also to the observation that experimental mole fraction of methylcyclopentadiene isomers ($C_5H_5CH_3$) is more than one order of magnitude higher than the model predicts (see Fig. 3). Such a huge difference of the mole fraction cannot only be explained by the fact that an estimated value for

the photoionization cross section was used. The almost exclusive pathway to methylcyclopentadiene in the reaction mechanism is the radical recombination $C_5H_5 + CH_3 = C_5H_5CH_3$. The photoelectron spectra of *m/z*=80 obtained from the flame with stoichiometry of 1.6 reveals by comparison with Franck-Condon simulations that three methylcyclopentadiene isomers are present in the flame (see Fig. S8). In the anisole mechanism of Wagnon et al. [16], 2-methylcyclopentadiene has the highest concentration during oxidation of anisole. The explanation for the higher concentration of the cyclopentadienyl radical in the leaner flame can be found from the reaction path analysis in Fig. 2 where the destruction rate of phenoxy radicals into benzoquinones ($C_6H_4O_2$) is 9.5% while it is only 3.7% in the richer flame. Evidence of the presence of benzoquinone in the product spectra was not found. Formation of *ortho*-benzoquinone was recently studied by the oxidation of *ortho*-hydroxyphenyl radicals in a slow-flow tube reactor [31]. Prompt CO elimination via ring opening and cyclisation yields cyclopentadienone (C_5H_4O) [31] which is also considered in the reaction mechanism. Cyclopentadienone was not found in detectable amounts in any of the flames. Conclusively, the formation of benzoquinone seems of minor importance for our investigated conditions. The presence of benzoquinone and cyclopentadienone in the oxidation of anisole were also not mentioned in the experiments of [11] and [13]. In conclusion, the pathway from phenoxy to cyclopentadiene (C_5H_6) and cyclopentadienyl radicals (C_5H_5) is more likely to account for the higher observed mole fractions of these two C_5 species.

In both flames, the phenol concentration is overpredicted by the model. Simulated peak mole fractions are two times higher than experimentally determined values. It seems that the phenol formation from the fuel or from the phenoxy is generally too strong in the model. This observation is supported by the fact that for the richer flame the benzaldehyde peak mole fraction is 1.8 times higher than the simulation predicts. In the mechanism of Nowakowska et al. [13], phenol is mainly formed from the phenoxy radical and not directly from the fuel. Other intermediate species found in higher concentrations and shown in Fig. 2 are acetylene, benzene, and formaldehyde. Good agreement is obtained for these species for both stoichiometries. Benzene, which is not shown in the

carbon flux diagram, is mainly formed in the leaner flame by *ipso* additions of hydrogen to phenol and benzaldehyde ($H + C_6H_5OH = C_6H_6 + OH$ and $H + C_6H_5CHO = C_6H_6 + HCO$). For the richer flame, formation of benzene from methylcyclopentadiene is the most relevant reaction ($H + C_5H_5CH_3 = H_2 + C_6H_6 + H$) and is consistent with the observed concentrations of these two species under the richer conditions. At temperatures below 950 K, the formation of benzene from anisole by *ipso* addition of H atoms is a minor route in the mechanism of Wagnon et al. [16]. The experimental peak mole fraction is 1.5 times higher than the model predicts for both methylcyclopentadiene and benzene as seen from Fig. 3. For anisole combustion, the C_5 species open a further formation pathway of aromatic compounds in addition to benzene formation from phenol and benzaldehyde. For example, recombination of the cyclopentadienyl radical to yield naphthalene, styrene formation from $C_5H_5 + C_3H_3 = C_6H_5C_2H_3$, or indene from reaction of cyclopentadienyl with cyclopentadiene [32].

3.3 Larger oxygenated species: the fate of guaiacol

In addition to the expected formation of oxygenates, for example, formaldehyde, acetaldehyde, and ketene, some larger oxygenated species are observed. Formation of phenol and benzaldehyde were already discussed in Section 3.2, but the reaction model also predicts cresols (methylphenols) from phenoxy radicals ($C_6H_5O + CH_3 = HOC_6H_4CH_3$) in significant amounts (peak mole fraction of $2 \cdot 10^{-3}$) in the richer flame. Cresols are isomers of anisole with higher ionization energy than anisole and there is no hint for cresols either in the photoelectron spectra or in the photoionization efficiency (PIE) curve. Due to the huge contribution of the anisole in the spectrum at *m/z*=108, their formation cannot be fully excluded. In the study of Nowakowska et al. [13], *ortho*- and *para*-cresol were identified in the pyrolysis and stoichiometric oxidation of anisole in a jet-stirred reactor.

A substance also related to lignin and not included in the model was observed at *m/z*=124. Guaiacol ($HOC_6H_4OCH_3$) also known as 2-methoxyphenol could be clearly identified in both flames. Identification was possible in both flames by comparison of measured PIE curves of *m/z*=124

with the reference of Hemberger et al. [33] (see Fig. S9 in the Supplementary Material). They have studied the catalytic pyrolysis of guaiacol by PEPICO and found fulvenone (C_5H_4CO) as the central reactive intermediate. Formation of guaiacol in the anisole flame may arise directly from the fuel by *ipso* addition of hydroxyl radicals ($C_6H_5OCH_3 + OH = HOC_6H_5OCH_3 + H$). The formation of *m*-guaiacol better known as 3-methoxyphenol was mentioned in the oxidation experiment of [13] and considered in their mechanism. Coeur-Tourneur et al. [34] studied rate coefficients of the gas phase reaction of OH radicals with anisole and methoxyphenols. They noted that the methoxy group in anisole activates *ortho* and *para* position towards electrophilic addition. As a result, the formation of the observed 2-methoxyphenol in our flames is more likely than 3-methoxyphenol. Even though an estimated photoionization cross section was used for quantification, comparability between the two stoichiometries is given because quantification of guaiacol was done from scans at nearly the same photon energy (9 and 9.05 eV). In the leaner flame, the peak mole fraction is 2.5 times higher (see Fig. S10). The presence of guaiacol enables formation of further oxygenated species analogous to anisole. For example, *ipso* additions with OH, H, or CH_3 would lead to catechol (*ortho*-benzenediol), phenol, and *ortho*-cresol, respectively, while unimolecular decomposition of the O–CH_3 group leads to reaction pathways analogous to phenoxy radicals (see scheme in Fig. S11). Fulvenone, which was identified during the pyrolysis in [33], was also clearly identified by comparison of the measured PIE curve of C_6H_4O in the leaner flame to measured PIE curve of fulvenone from Hemberger et al. [33] (see Fig. S12). Oxygenated species with still higher masses, e.g., $C_{12}H_{10}O$ on *m/z*=170, than guaiacol could also be observed but lack of known ionization energies makes identification difficult.

4. Conclusions

The aromatic ring in anisole in combination with the methoxy group makes it the simplest model compound for lignin. The combustion of anisole in two laminar, premixed, fuel-rich flames was investigated by synchrotron-based photoionization mass spectrometry. Isomer-resolved speciation data is provided and give insights into the reaction kinetics of anisole in a flame environment. The

experimental results were compared to predictions of a comprehensive reaction mechanism from the literature suitable for many hydrocarbon and oxygenated fuels. General shape and trends of the mole fraction profiles of the flames with two different equivalence ratios are well-predicted by the model of Ranzi et al. [25]. Considering the uncertainty of the experiment and the fact that the reaction mechanism was used without any adaptations, reasonable agreement for many combustion intermediates is found. As expected from the weak bond of the $O–CH_3$ group, decomposition of anisole to phenoxy and methyl radicals is strongly favored, especially for the richer condition and at higher temperatures. For the leaner flame and close to the burner at moderate temperatures, benzaldehyde formation becomes a stronger pathway. Five-membered ring species (C_5H_5, C_5H_6, and $C_5H_5CH_3$) play a significant role in the anisole combustion by providing a formation way of aromatic compounds without benzene involved. Guaiacol is an oxygenated compound produced from buildup reactions and is also formed during biomass oxidation and pyrolysis. Direct formation from anisole by *ipso* addition reaction with OH may be a formation pathway of this compound. The presence of guaiacol can explain the formation of other oxygenated species, e.g., fulvenone (C_5H_4CO), which are rather unusual in the combustion of conventional hydrocarbons and opens new reaction pathways beyond the phenoxy radical route and may result in unexpected pollutant emission.

Acknowledgments

All authors thank the Deutsche Forschungsgemeinschaft for financial support under contract KA3871/3-1 and KO4786/2-1. Patrick Hemberger also thanks the Swiss Federal Office of Energy for financial support under contract SI/501269-01. Experiments were performed at the SLS of the Paul Scherrer Institute and the ALS of the Berkeley Lab. We thank Dr. Nils Hansen and Paul Fugazzi from Sandia National Laboratories for experimental research support and technical assistance. The ALS is supported by the Director, Office of Science, Office of Basic Energy Sciences, of the U.S. Department of Energy under Contract No. DEAC02-05CH11231.

References

[1] A. Pandey, C. Larroche, S.C. Ricke, C.-G. Dussap, E. Gnansounou, Biofuels: Alternative Feedstocks and Conversion Processes, Academic Press, Amsterdam, 2011.

[2] M. Boot, Benzenoids, in: M. Boot (Ed.), Biofuels from lignocellulosic biomass: Innovations beyond bioethanol, Wiley-VCH, Weinheim, 2016, pp. 159-188.

[3] L. Zhou, M.D. Boot, B.H. Johansson, J.J.E. Reijnders, Fuel, 115 (2014) 469-478.

[4] M. Tian, R.L. McCormick, M.A. Ratcliff, J. Luecke, J. Yanowitz, P.A. Glaude, M. Cuijpers, M.D. Boot, Fuel, 189 (2017) 284-292.

[5] M.F.R. Mulcahy, B.G. Tucker, D.J. Williams, J.R. Wilmshurst, Aust. J. Chem., 20 (1967) 1155-1171.

[6] R.H. Schlosberg, P.F. Szajowski, G.D. Dupre, J.A. Danik, A. Kurs, T.R. Ashe, W.I. Olmstead, Fuel, 62 (1983) 690-694.

[7] C.-Y. Lin, M.C. Lin, Int. J. Chem. Kinet., 17 (1985) 1025-1028.

[8] C.-Y. Lin, M.C. Lin, J. Phys. Chem., 90 (1986) 425-431.

[9] J.C. Mackie, K.R. Doolan, P.F. Nelson, J. Phys. Chem., 93 (1989) 664-670.

[10] I. Arends, R. Louw, P. Mulder, J. Phys. Chem., 97 (1993) 7914-7925.

[11] M. Pecullan, K. Brezinsky, I. Glassman, J. Phys. Chem. A, 101 (1997) 3305-3316.

[12] A.M. Scheer, C. Mukarakate, D.J. Robichaud, G.B. Ellison, M.R. Nimlos, J. Phys. Chem. A, 114 (2010) 9043-9056.

[13] M. Nowakowska, O. Herbinet, A. Dufour, P.A. Glaude, Combust. Flame, 161 (2014) 1474-1488.

[14] B. Husson, M. Ferrari, O. Herbinet, S.S. Ahmed, P.A. Glaude, F. Battin-Leclerc, Proc. Combust. Inst., 34 (2013) 325-333.

[15] B. Shu, J. Herzler, S. Peukert, M. Fikri, C. Schulz, Int. J. Chem. Kinet., 49 (2017) 656-667.

[16] S.W. Wagnon, S. Thion, E.J.K. Nilsson, M. Mehl, Z. Serinyel, K. Zhang, P. Dagaut, A.A. Konnov, G. Dayma, W.J. Pitz, Combust. Flame, 189 (2018) 325-336.

[17] N. Hansen, T.A. Cool, P.R. Westmoreland, K. Kohse-Höinghaus, Prog. Energy Combust. Sci., 35 (2009) 168-191.

[18] E.L. Knuth, Combust. Flame, 103 (1995) 171-180.

[19] T. Bierkandt, P. Hemberger, P. Oßwald, M. Köhler, T. Kasper, Proc. Combust. Inst., 36 (2017) 1223-1232.

[20] T.A. Cool, A. McIlroy, F. Qi, P.R. Westmoreland, L. Poisson, D.S. Peterka, M. Ahmed, Rev. Sci. Instrum., 76 (2005) 094102/1-094102/7.

[21] A. Bodi, M. Johnson, T. Gerber, Z. Gengeliczki, B. Sztáray, T. Baer, Rev. Sci. Instrum., 80 (2009) 034101/1-034101/7.

[22] P. Oßwald, P. Hemberger, T. Bierkandt, E. Akyildiz, M. Köhler, A. Bodi, T. Gerber, T. Kasper, Rev. Sci. Instrum., 85 (2014) 025101/1-025101/11.

[23] P. Oßwald, K. Kohse-Höinghaus, U. Struckmeier, T. Zeuch, L. Seidel, L. Leon, F. Mauss, Z. Phys. Chem., 225 (2011) 1029-1054.

[24] F.N. Egolfopoulos, N. Hansen, Y. Ju, K. Kohse-Höinghaus, C.K. Law, F. Qi, Prog. Energy Combust. Sci., 43 (2014) 36-67.

[25] E. Ranzi, A. Frassoldati, R. Grana, A. Cuoci, T. Faravelli, A.P. Kelley, C.K. Law, Prog. Energy Combust. Sci., 38 (2012) 468-501.

[26] Chemical Workbench, http://www.kintechlab.com/, Version 4.1.19528, 2017.

[27] E.B. Hemings, G. Bozzano, M. Dente, E. Ranzi, Chem. Eng. Trans., 24 (2011) 61-66.

[28] P.E.A. Debiagi, G. Gentile, M. Pelucchi, A. Frassoldati, A. Cuoci, T. Faravelli, E. Ranzi, Biomass Bioenerg., 93 (2016) 60-71.

[29] H. Xu, S.T. Pratt, J. Phys. Chem. A, 117 (2013) 12075-12081.

[30] A.J. Colussi, F. Zabel, S.W. Benson, Int. J. Chem. Kinet., 9 (1977) 161-178.

[31] M.B. Prendergast, B.B. Kirk, J.D. Savee, D.L. Osborn, C.A. Taatjes, K.S. Masters, S.J. Blanksby, G. da Silva, A.J. Trevitt, Phys. Chem. Chem. Phys., 18 (2016) 4320-4332.

[32] C. Cavallotti, D. Polino, A. Frassoldati, E. Ranzi, J. Phys. Chem. A, 116 (2012) 3313-3324.

[33] P. Hemberger, V.B.F. Custodis, A. Bodi, T. Gerber, J.A. van Bokhoven, Nat. Commun., 8 (2017) 15946/1-15946/9.

[34] C. Coeur-Tourneur, A. Cassez, J.C. Wenger, J. Phys. Chem. A, 114 (2010) 11645-11650.

List of supplemental material:

PDF document includes additional information about the experiment, the data reduction, Table S1, and supporting figures.

An Excel sheet includes the temperature profile used for kinetic modeling and the calculated mole fraction profiles of both flames.

List of figure captions:

Fig. 1. Main species mole fractions and temperature profile of the anisole flame with stoichiometry of 1.6 measured at the SLS. Symbols: experimental data; solid lines: modeling results; dashed line: temperature profile.

Fig. 2. Fig. 2. Reaction pathways of total carbon flux in the entire flames. Solid arrows (blue): Φ=1.2; dashed arrows (red): Φ=1.6.

Fig. 3. Mole fraction profiles of some stable intermediate and radical species founded in higher concentration. Symbols: experimental data; solid lines: modeling results.